Materials Today Bio 18 (2023) 100550

Contents lists available at ScienceDirect

Materials Today Bio

journal homepage: www.journals.elsevier.com/materials-today-bio

Bioprinting a skin patch with dual-crosslinked gelatin (GelMA) and silk fibroin (SilMA): An approach to accelerating cutaneous wound healing

Lei Xu [a,b,1], Zhiqiang Zhang [a,b,1], Adam M. Jorgensen [c], Yuan Yang [d], Qianheng Jin [b], Guangliang Zhang [b], Gaobiao Cao [b], Yi Fu [e], Weixin Zhao [c], Jihui Ju [b,**], Ruixing Hou [b,*]

[a] Suzhou Medical College of Soochow University, Suzhou, 215123, China
[b] Department of Hand Surgery, Suzhou Ruihua Orthopaedic Hospital, Suzhou, 215104, China
[c] Wake Forest Institute for Regenerative Medicine, Winston-Salem, NC, 27257, USA
[d] Hospital of Medical College of Yangzhou University, Yangzhou, China
[e] Department of Human Anatomy, Histology and Embryology, School of Biology and Basic Medical Sciences, Soochow University, Suzhou, 215123, China

ARTICLE INFO

Keywords:
Dual-cross-linked hydrogel
Gelatin
Silk fibroin
3D bioprinting
Wound healing

ABSTRACT

Clinical settings often face significant obstacles in treating large acute wounds. The alternative of therapeutic approach is needed urgently. Hydrogels derived from natural or synthetic materials may be designed to perform a variety of functions for promoting wound healing. Herein, a 3D bioprinted hydrogel patch is designed for accelerating acute wound healing, which is fabricated with methacryloyl-substituted gelatin (GelMA) and silk fibroin (SilMA) dual-cross-linked by ultraviolet (UV) light. The GelMA with added silk fibroin (GelSilMA) shows improved biodegradation and mechanical properties. Furthermore, SilMA hydrogel can maintain a moisturized healing environment in wound area persistently with adequate degradation capacity. In vivo, GelSilMA (G-S) hydrogel can help to speed wound closure by the improved microenvironment for epidermal tissue regeneration and endogenous collagen generation accordingly. In summary, the G-S hydrogel patch can accelerate acute wound healing efficiently in a relatively simple and inexpensive manner.

1. Introduction

Skin serves as a primary barrier between the inner and outer worlds of an individual. Extensive skin damage may occur when an acute injury happens. The serious skin wound that opens to the air for a long time can result in various health consequences, including shock, systemic infections, and even death [1]. Furthermore, acute wounds that are not treated properly can develop into chronic wounds, which prolongs the duration of the disease and increases the difficulty of treatment. To date, autologous skin grafting is the most effective technique for treating large skin defects [2]. Unfortunately, the limited availability of autologous skin grafts can significantly delay the treatment times or even result in uncompleted coverage of the wounded area, as well as add additional skin injury due to harvesting skin grafts [3]. Cadaveric skin transplantation is an alternative strategy. However, this kind of allogenic skin is usually from the cadavers with aging and unhealthy history, which is associated with the infection, immune rejection, and ethical issues [4]. The tissue engineering strategies are intended to accelerate wound healing by providing the coverage of wound bed with artificial matrix, which allows skin cells such as keratinocytes and dermal fibroblasts to migrate and proliferate in the wound area.

Currently, three-dimensional (3D) bioprinting has emerged as an efficient technique for the healing of cutaneous wounds [5–7]. As a result of its accessibility, cost-effectiveness and ability to reproduce tissue complexity, extrusion-based bioprinting integrated with cell-loaded hydrogel has become the most suitable technique for treating cutaneous wounds. To fabricate geometrically well-defined 3D complex structures, extrusion-based bioprinter delivers uninterrupted arrays of hydrogel on a free-moving container in predesigned layers [8]. It is imperative to develop the skin-specific hydrogel that is compatible with skin-related cells and promotes the cell migration, growth, and proliferation. However, current extrusion-based hydrogels are limited by certain bio-physical properties (mechanical, structural, or biodegradable) that are not conducive to skin regeneration, and a compromise is

* Corresponding author.
** Corresponding author.
E-mail addresses: jjh2020@suda.edu.cn (J. Ju), hrx2020@suda.edu.cn (R. Hou).
[1] These authors contributed equally.

https://doi.org/10.1016/j.mtbio.2023.100550
Received 14 October 2022; Received in revised form 15 December 2022; Accepted 11 January 2023
Available online 14 January 2023

usually needed between hydrogel printability and cellular compatibility [9]. Ideally, the skin-specific hydrogel should exhibit biological characterizes of supporting cells migration, adhesion, and proliferation, as well comply with appropriate mechanical and degradation properties [10].

The hydrogels derived from natural sources have been considered attractive candidates for engineering dermis due to their unique combination of biological and physical properties. The gelatin as one of natural biomaterials is commonly used to synthesize hydrogels. Gelatin modified with methacrylamide groups (GelMA) retains the properties of the natural material and allows it to be solidified permanently in the gelatinous form. The GelMA scaffold contains several peptides that closely mimic the properties of native extracellular matrix (ECM), including arginine-glycine-aspartic acid (RGD) that promotes cell attachment and activated matrix metalloprotease (MMP) that allows cells to multiply and spread in the scaffold [11,12]. Furthermore, GelMA has the desirable thermosensitive properties of being solid below 25 °C and becoming colloidal above 37 °C, which make it suitable for 3D extrusion bioprinting [13]. Due to its low cytotoxicity, low concentration GelMA (i.e., ≤5% w/v%) in the hydrogel has been suggested to for keeping cell survival [14]. Stratesteffen et al. [15] found that relatively low concentrations of GelMA (4%) may be more suitable for vascular endothelial cell migration and angiogenesis, which play an important role in wound healing through proliferation and remodeling processes. However, the hydrogel with low concentration GelMA exhibits the rapid degradation and poor mechanical properties [16]. The solution to the improvement of GelMA is needed urgently. Therefore, we are looking for an additive that could enhance the degrading and mechanical properties of GelMA at low concentration, based on that a new formular of GelMA would benefit skin regeneration.

Silk Fibroin (SF) produced by Bombyx mori is FDA-approved for use as a drug delivery system and surgical suture. Due to its hydrophobicity, considerable hydrogen bonding and high protein crystallinity provided by β-sheet crystals, SF is stronger and longer-lasting than other natural materials in vivo [17,18]. In spite of its good elasticity, SF is difficult to fully photocrosslink [19]. A modification of SF with glycidyl methacrylate (GMA) results in silk fibroin glycidyl methacrylate (SilMA), which increases the stability of silk fibroin hydrogel and the degree of photocrosslinking [20]. It has been demonstrated that methacrylated silk fibroin (SilMA) exhibits extraordinary biological characteristics that facilitate wound reconstruction, such as enhanced proliferation and matrix deposition of fibroblasts, robust mechanical properties, and minimal inflammatory response [21]. Nevertheless, the SF obtained through standard processing techniques is of low concentrations (6% w/v)) and low viscosity that makes it ineligible for 3D bioprinting with extrusion manner. Furthermore, the absence of cell binding sequences arginine-glycine-aspartic acid (RGD) in SilMA makes it incompatible with cellular attachment on its surface [22]. Though SilMA cannot meet the needs of regenerating skin by itself through extrusion bioprinting, a mixture of GelMA at a low concentrations (≤ 5% w/v) and SilMA at a designed concentration becomes an ideal composite hydrogel (G-S) which could be fabricated through extrusion bioprinting and has good biological and mechanical properties. Recently, relatively high concentrations of GelMA (10% w/v) blends with SilMA have been reported for extrusion-based 3D printing in wound healing [19,23]. However, Yue et al. [24]discovered that the concentration of 5% (w/v) GelMA might be too high to allow cell spreading, cell migration, communication between cells, and gaining sufficient supply of oxygen and nutrients. Therefore, a hybrid hydrogel containing a low concentration of GelMA may be more appropriate for engineering skin tissue.

In this study, we present a modified hybrid hydrogel to accelerate cutaneous wound healing with 3D bioprinting technology. G-S was synthesized by incorporating reactive methacryloyl groups into gelatin and silk fibroin to produce a dual-crosslinked composite hydrogel (Fig. 1A) for the fabrication of skin repair patch by 3D bioprinting. The SilMA concentration within G-S hydrogel was optimized by testing cell adhesion, proliferation, migration, and mechanical properties in vitro. In comparison with a single network structure of GelMA and SilMA, the G-S hydrogel was further optimized in terms of printability, mechanical properties, degradation rate, swelling rate, and capacity to heal acute wounds. As a proof-of-concept study, a normal full-thickness wound model has been established in a mouse model to evaluate the in vivo healing efficacy of G-S hydrogel (Fig. 1B). To our knowledge, this work is a novel advancement in the application of tunable GelMA and SilMA properties for enhanced cell attachment, proliferation, and function in a bioengineered skin patch.

2. Material and methods

2.1. Synthesis of gelatin methacryloyl

In accordance with the previous description, gelatin methacryloyl (GelMA) was synthesized. (Fig. 1). Briefly, Gelatin (G1890, Sigma-Aldrich, USA) was dissolved in 50 ml of 0.25 M carbonate-bicarbonate buffer (pH 9, room temperature) for 1 h at 55 °C, followed by adding 0.5 ml of methacrylic anhydride (276 685, Sigma-Aldrich, USA) and stirring for 3 h at 55 °C. To stop the reaction, 80 ml of Dulbecco's phosphate buffered saline (DPBS) (SH30028.02, HyCloneTM, USA; pH 7–7.6) was added, and then dialyzed by distilled water for 1 week at 37 °C. The obtained GelMA was frozen and lyophilized for further use.

2.2. ^1H nuclear magnetic resonance (^1H NMR)

The degree of functionalization of GelMA was determined by ^1H NMR ((^1H NMR, Bruker, Billerica, MA) as described previously. In short, GelMA was dissolved in 15 mg per ml of D_2O water at 50 °C until completely dissolved. At 400 MHz, the ^1H NMR spectrometer was used to conduct the spectroscopy at room temperature. Methacrylate double bonds exhibit hydrogen peaks of between 5.5 and 5.7 ppm, which represents GelMA, but not gelatin.

2.3. TNBS assay

Assays for the determination of free amine levels after GelMA synthesis were performed using a 2, 4, 6-trinitrobenzenesulfonic acid (TNBS) assay. In short, GelMA was dissolved in 0.1 M sodium bicarbonate solution (PH = 8.5) to achieve a concentration of 200 μm L^{-1} [25]. The sample solution was then diluted with 250 mL TNBS and incubated at 37 °C for 2 h following dissolution. A mixture of 250 μL 10% SDS, and then 125 μL of 1 N hydrochloric acid (HCl) was used to stop the reaction. With the aid of a spectrophotometer set at 335 nm, the optical density was determined. The Gelatin served as a control. Based on the formula below, the degree of methacrylation of GelMA was calculated.

Degree of methacrylation (%) = (1- OD of GelMA/OD of Gelatin) × 100, where OD stands for the optical density.

2.4. Preparation of GelMA, SilMA, and G-S hydrogels

In a 5 mL vial (SenFei Lab, Yancheng, China), 40 mg/mL GelMA was dissolved in 0.25% (w/v) LAP (EFL, Suzhou, China) solution to produce a high viscosity solution. A homogeneous GelMA hydrogel was obtained by rumbling the high viscosity solution at 20 rpm, 37 °C for1 h. SilMA was purchased from EFL (EFL-SilMA-001, Suzhou, China). For the SilMA hydrogel preparation, 40 mg Gelatin was dissolved into 1 ml 0.25% LAP with a shaker set at 20 rpm and 37 °C for 1 h. Subsequently, 80 mg/mL SilMA was added into the vial and kept on shaker for an additional 1 h. The preparation of G-S hydrogel is similar to that of SilMA hydrogel. The lyophilized GelMA was added into LAP solution to dissolve completely, and then SilMA was added. Once fully dissolved, the warm macromeres were loaded into syringe of Bioprinter (Bio X™, Cellink, Sweden).

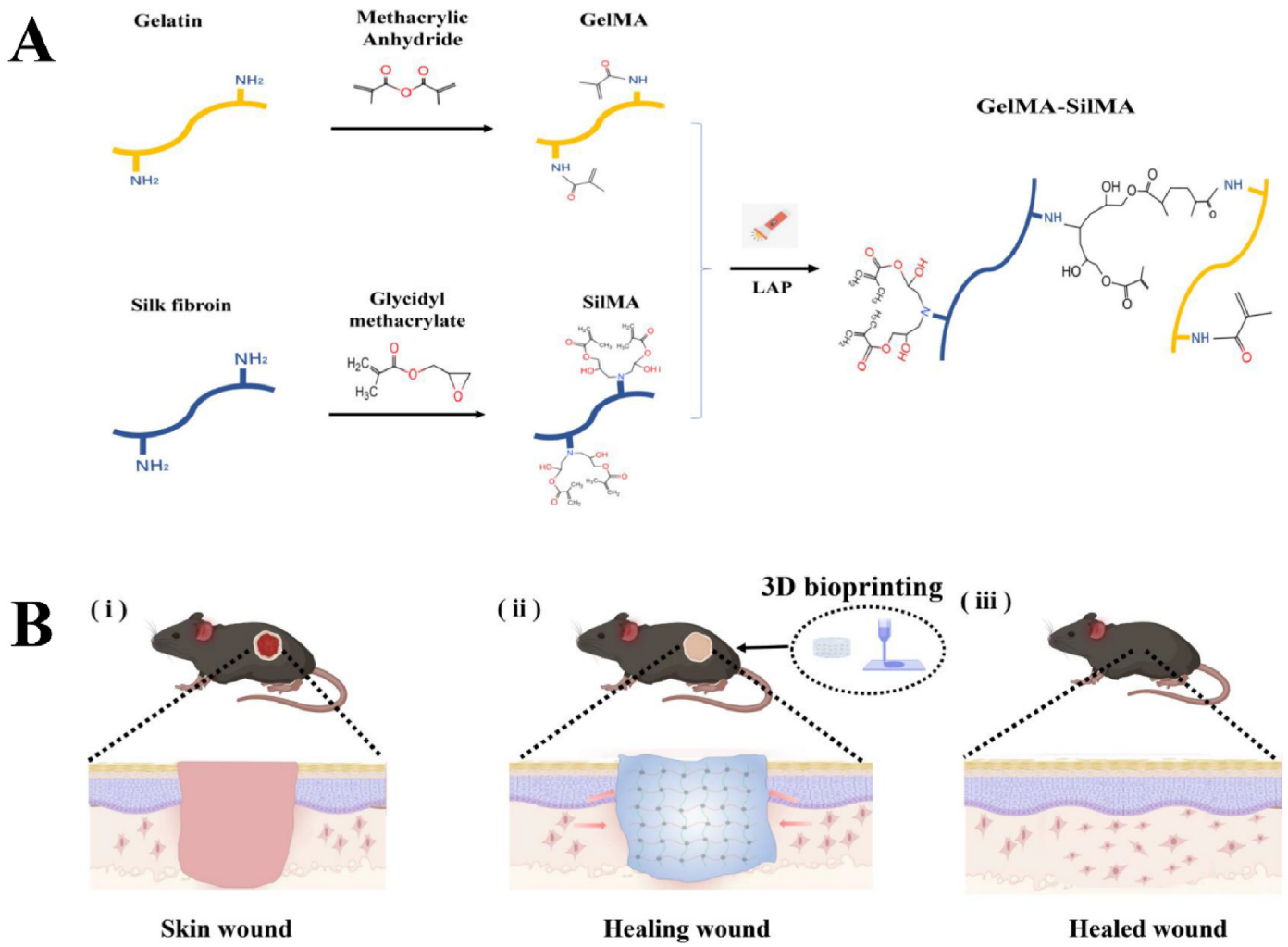

Fig. 1. (A) Schematic for preparing GelMA, SilMA, and dual-crosslinked G-S hydrogel patch. (B) Schematic illustration of mechanism of dual-cross-linked GelSilMA hydrogel patch promotes acute wound healing.

2.5. Microstructure of hydrogels

The microstructure of hydrogels was observed by scanning electron microscopy (SEM) (Gemini 300, ZEISS, Germany). Briefly, the 3D bioprinted constructs were crosslinked by UV (UVP Crosslinker CL-1000 L, Analytik Jena, USA) with an intensity of 25 mW/cm^2 for 30 s, and then immersed in deionized water overnight at 37 °C. Hydrogel samples were lyophilized after being frozen at −80 °C for 2 days. Subsequently, gold was sputtered onto the cross sections of the constructs for 2 min at 15 mA, and the cross-sections were observed under SEM at a 5 kV with 200 × magnification. NIH Image J (NIH Image, Bethesda, Maryland, USA) was used to determine the pore sizes and to examine the pore structure in the matrices (n = 3 per group).

2.6. Mechanical property test of the hydrogels

The rheology of the hydrogels was tested with TA DHR -2 rheometer (TA Instruments, USA) using 8 mm steel parallel plate geometry at 25 °C. In short, On the rheometer stage, the construct sample was loaded, and the 8 mm steel plate geometry was lowered until contacting with the surface of the sample. Further geometry lowering was completed until the axial force on the instrument showed 0.02 N. A shear stress sweep test was performed with strain equal to 1.0% and a frequency of 1 Hz to measure the storage modulus (G′) and loss modulus (G″) of each hydrogel. At the 30th second, UV irradiation was applied for 30 s during a total of 120 s test time. Three measurements per construct were performed. For different skin patches with different concentrations and proportion, the rheological assessments were done separately.

Viscosity of composite hydrogel solutions (G:S = 1:0, G:S = 1:1, G:S = 1:2, and G:S = 1:3) was analyzed separately with TA DHR -2 rheometer using a 40 mm steel parallel plate geometry at 18 °C. The gap between the surface of hydrogel solution and the plate was 0.4 mm. Tests were performed at shear rates of 0.01–100 s^{-1}, which corresponds to the range of shear rates that are normally encountered when extrusion bioprinting is used [26]. Each assessment was conducted in three copies.

2.7. Swelling behavior

Swelling behavior of bioprinted patches made with composite hydrogels (G:S = 1:0, G:S = 1:1, G:S = 1:2, and G:S = 1:3) were evaluated separately. The bioprinted patches (8 mm in diameter and 400 μm in thickness) were immersed in PBS for 24 h post-crosslinking, frozen overnight at −80 °C, lyophilized for 2 days, and weighed (W_0). The lyophilized samples were immersed in PBS at 37 °C following the predetermined time interval and blotted with filter paper to remove the remaining water. And then the swelling weight was recorded (W_t) . The swelling ratio of hydrogel was calculated by the equation as:

$$\text{Swelling ratio } (\%) = (W_t - W_0) \ / \ W_0 \times 100\% \ (n = 3 \text{ per group}).$$

2.8. Degradation behavior

The degradations of the printed hydrogel patches in vitro were analyzed by immersing equal volumes of hydrogel blocks in 1.5 mL PBS containing 1.25 U/mL of type II collagenase (C6885-500 MG, Sigma-Aldrich, USA) at 37 °C for 14 days, and the immersing media were refreshed every 3 days to maintain the enzyme activity. The printed hydrogel patches were rinsed with deionized water at each time point and then freeze-dried for three days. The weights of dried samples were recorded (W_t) at each time point, and the initial weight of the sample was recorded as W_0. The degradation ratio of printed patch was calculated as follows:

$$\text{Degradation ratio } (\%) = (W_t - W_0) \ / \ W_0 \times 100\% \ (n = 3 \text{ per group}).$$

2.9. Isolation of fibroblasts

Skin biopsies were conducted in male C57BL/6 mice. After shaving off the hair from the mice's dorsum, a biopsy specimen of 3 × 3 cm^2 was taken. The skin sample was washed 3 times with PBS + penicillin-streptomycin solution lasting for 5 min. The skin tissue was then cut into pieces of 0.5 × 0.5 cm^2 with sterile scissors and digested with neutral protease for 16–18 h. The epidermis was separated from the dermis with sterile forceps. The dermis was minced, incubated in 2 mg/ml of type II collagenase (dermis volume to collagenase volume = 1:4), and kept in a shaker (37 °C, 140 rpm) for 4 h at 37 °C to isolate the fibroblasts. The final solution was filtered through a 75 μm filter and then centrifuged at 1500 rpm for 5 min. Isolated cells were cultured in a 6 cm tissue culture dish containing 8 mL of Dulbecco's modified Eagle medium (DMEM; Gibco, USA) with 10% fetal bovine serum (Gibco, USA). The cells were identified with α-actin antibody staining (Santa Cruz, Dallas, TX, USA). The cells within 5 passages were used for all the experiments.

2.10. Cell adhesion assessment

Briefly [27], 25 μL of hydrogel was crosslinked on the bottom of a 24-well plate and 3 × 10^5 Fibroblast cells were seeded on top of the gel and cultured for 4 h under aseptic conditions. As a positive control, the same number of Fibroblast cells were seeded onto a 24-well TCP cell culture dish. After 4 h, the medium was gently aspirated from the well, and then the seeded cells were gently washed twice with PBS. The cells were stained with DAPI dye for 5 min, and then viewed under an inverted microscope.

2.11. Cell migration assessment

The scratch experiment was conducted to determine how hydrogel affects the migration of fibroblasts. In a 6-well plate coated with GelMA or GelSilMA hydrogel, 2 × 10^6 fibroblast cells per well were cultured for 24 h. Following the removal of the medium, a scratch was made at the bottom of each well with the same width. An inverted microscope was used to observe the cells after they had been incubated a certain amount of time, and images were taken to monitor the migration of the cells onto the scratched surface. NIH Image J was used to determine the scratched area. (n = 3 per group).

2.12. 3D bioprinting of skin patch

For bioprinting the skin patch, one syringe was utilized to load Fibroblast-laden hydrogel and 400 μm nozzle was chosen. Prior to bioprinting, a customized printing code was developed that enables the bioprinter to print a round shape with the fibroblast-laden hydrogel in monolayer. The 3D bioprinting parameters and working condition were as follows: 1) The density of fibroblasts was 20 × 10^6 per ml. 2) The pressure and velocity of dispensing were 100 kPa and 90 mm per minute, respectively. 3) The bioprinter chamber was maintained at 18 °C using an integrated cooling system.

2.13. Cell viability assessment

The viability of the 3D bioprinted skin patch was evaluated by the Live/Dead test. Specifically, samples were collected and washed 3 times with PBS prior to incubating with staining solution containing 0.5 μL of calcein-AM and 2 μL of ethidium homodimer (L3224, Invitrogen, USA) at 37 °C for 45 min. The dead and living cells were assessed by laser confocal microscopy (Zeiss LSM 880, Oberkochen, Germany). NIH Image J software was used to analyze six random views of each sample and calculate the viability as a percentage of the live cells in the total number of cells per area.

2.14. Cell proliferation assessment

The proliferation of fibroblast cells in printed skin patches was quantified by 3-(4, 5-dimethylthiazol-2-yl)-2, 5-diphenyl tetrazolium bromide (MTT) solution (0.5% w/v) according to manufacturer's instruction. Briefly, in 24-well plates, the original culture medium was removed and replaced with 900 μL fresh culture medium and 100 μL MTT solution (M2128, Sigma, USA). Upon incubation for 4 h at 37 °C, the solution was removed. After that, 500 μL of dimethylsulfoxide solution (DMSO, D2650, Sigma-Aldrich, USA) was added to the solution, which was shaken horizontally at 37 °C for 30 min. The absorbance at 570 nm was measured using the SpectraMax M5 with 100 μL of solution per well.

2.15. Wound healing assessment

The male C57BL/6 mice were purchased from Yangzhou University Center for Comparative Medicine. All animals were housed in facilities meeting SPF levels, in which light and darkness were alternated for a 12-h period. Following anesthesia, skin biopsy punches created two 8 mm diameter full thickness wounds on the shaved and sterilized dorsum in both side of the spinal, one of that was for experimental group and the other of that was set as control group. The C57BL/6 mice were divided randomly into three groups of GelMA hydrogel, SilMA hydrogel, and G-S hydrogel, respectively. At 0, 3, 7, 9, and 12 days after the operation, images of the wound were taken, which were analyzed using Image J software to evaluate the healing. The wound healing ratio was calculated by the equation as showing below, where H_0 and H_t stand for the unhealed areas on day 0 and predetermined time. Wound healing ratio (%) = $(1 - H_t/H_0) \times 100\%$ (n = 3 per group).

2.16. Histological and immunofluorescent analysis

Regenerated dorsal skins were collected on the 7th and 12th day after the implantation. Tissues were processed for paraffin section and cryosection. For H&E Staining, slides were soaked in xylene for 20 min before being washed with ethanol gradient solutions. Following immersed in hematoxylin for 5 min. Afterwards, the slides were immersed in eosin staining for 2 min, dehydrated in absolute ethanol, and gotten transparent in xylene for 15 min. Ultimately, neutral resin was applied, and the slides were sealed. For Masson's Trichrome staining, the Masson's Trichrome Staining Kit (G1340, Beijin Solarbio Science & Technology Co., Ltd) was performed following the manufacturer's instruction. Briefly, the slides were stained with Weigert's iron hematoxylin solution for 10 min. In the following steps, the slides were rinsed with water and immersed in the differentiation solution for 3 s, stained with Ponceau acid fuchsin for 5 min, then immersed in a solution of phosphomolybdic acid for 1 min, and stained with aniline blue for 5 min. A 1% glacial acetic acid solution was used to differentiate the sections, which were then dehydrated, mounted, and sealed. For immunohistochemistry staining, the slides were heated in an oven at 60 °C for 2 h,

deparaffinized in xylene, rehydrated in an ethanol gradient, and then incubated in an antigen retrieval solution (citric acid 0.4 g/L and trisodium citrate 3 g/L) for 20 min. Incubation was performed with a peroxidase inhibitor (MXB, Fuzhou, China) for 10 min, followed by blocking with 10% goat serum for 1 h. Then, the slides were incubated with the primary antibody against PCNA (Abcam, Cambridge, UK) at 4 °C overnight, rinsed with PBS and incubated with the secondary antibody from MaxVison™ HRP-Polymer anti-Rabbit IHC Kit (MXB, Fuzhou, China) for 1 h. Upon washing with PBS, sections were incubated with diaminobezidin (MXB, Fuzhou, China), counterstained with hematoxylin and viewed under a light microscopy (TH4 - 200, Olympus Corporation, Japan). For immunofluorescence staining, the samples were fixed with 4% (v/v) paraformaldehyde and permeabilized with 0.2% (v/v) Triton X-100. The slides were incubated with mouse anti-mouse CD31(1:250, Abcam, USA) overnight at 4 °C and then a secondary antibody (1:50, Bioworld Technology, MN, USA). Finally, the nuclei were stained with DAPI (1:1000, D3571, Life Tech, USA) for 5 min at room temperature. The slides were viewed by laser confocal microscopy (Zeiss LSM 880, Oberkochen, Germany). The soft of Image J (NIH Image, Bethesda, Maryland, USA) was used to analyze the positive immunohistochemical and immunofluorescence signals.

3. Results and discussion

3.1. Fabrication and characterization of G-S hydrogel

To simulate a natural ECM, synthetic materials might be suboptimal [28]. The development of engineering scaffolds using the materials derived from natural resources has received increased attention for repairing damaged tissues [29]. In this study, a photocrosslinkable gelatin prepolymer (GelMA) was synthesized by introducing reactive methacrylate group into gelatin. As shown in Fig. 2A, the success of the conjugation was confirmed by proton nuclear magnetic resonance (^{1}H NMR). GelMA, but not gelatin, shows peaks between 5.5 ppm and 5.7 ppm of the hydrogens in the double bond of methacrylate groups. According to prior reports, the synthesized GelMA had a level of methacrylamide modification of 79.6 ± 3.0%, which was in accordance with previous reports (data not shown) [13]. The peptide sequences in GelMA closely resemble those found in the native extracellular matrix (ECM), including RGD that promotes cell attachments, and MMP that allows cells to proliferate and grow in the scaffolds [30,31]. The GelMA network was used to compensate the lack of polysaccharide for cell adhesion. However, the 3D printed structure using GelMA at low concentration (≤5% w/v %) alone degrades rapidly after being implanted in vivo [16]. To overcome the shortage, a mixture of GelMA with other polymers was considered to improve the performance of the material. SilMA was chosen as another crosslinkable network to compensate for the weak mechanical performance and rapid degradation of GelMA. By incorporating reactive methacrylates into silk fibroin, a photocrosslinkable silk fibroin prepolymer was synthesized. GelMA and SilMA can be mixed to form a dual-crosslinked G-S hydrogel patch through 3D bioprinting under ultraviolet (UV) exposure (Fig. 2B). In this study, Gelatin-based bioink (GelMA) was produced using a methacrylic anhydride (MA)-based methylation process during the fabrication of gelatin solution, while SilMA was synthesized by glycidyl methacrylate (GMA) methacrylate during the fabrication of silk fibroin solution. Although these two

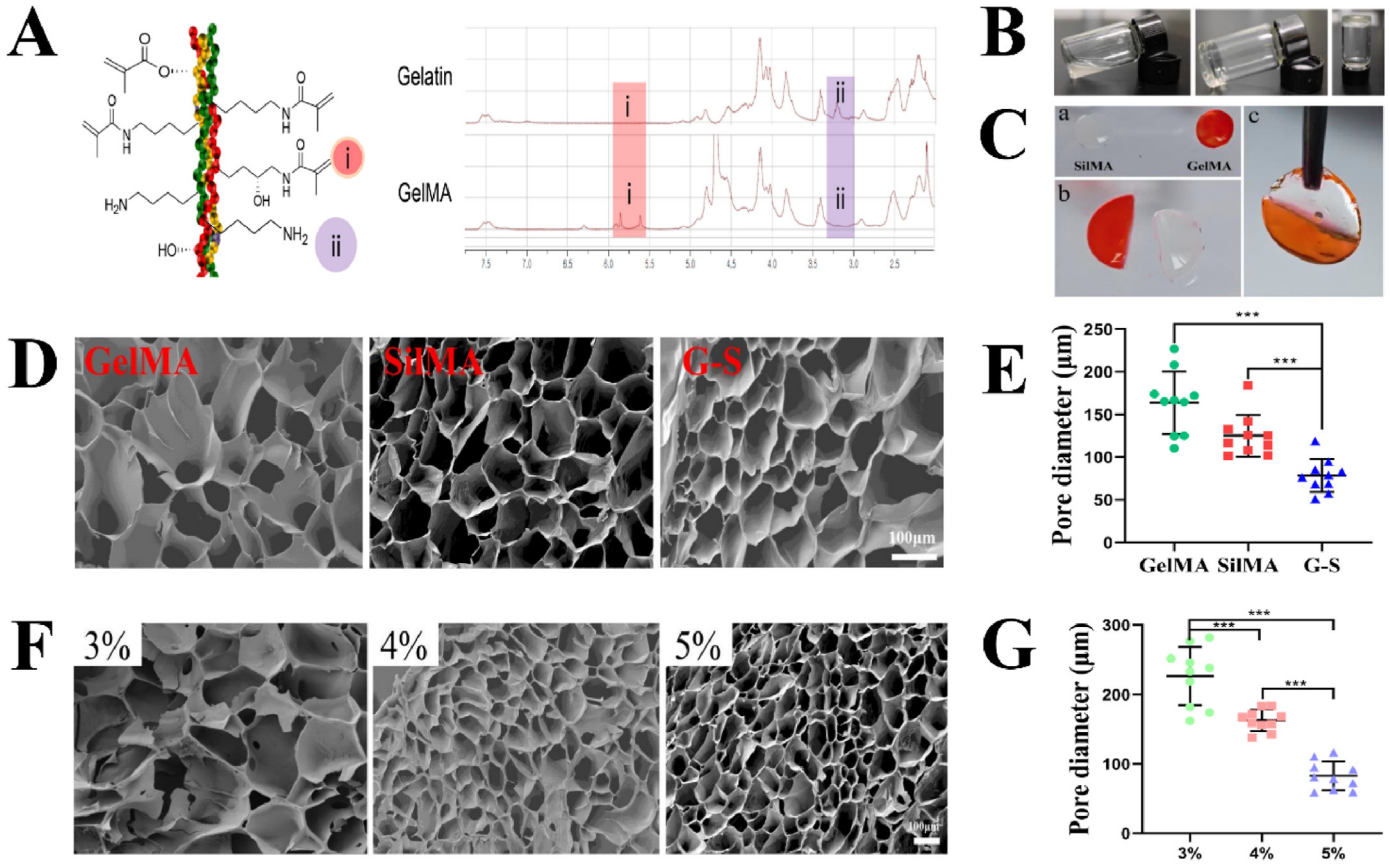

Fig. 2. (A) Synthesis and confirmation of methacrylated gelatin (GelMA). (B) Gross observation of G-S hydrogel before and after UV crosslinking. (C) Schematic illustration of GelMA and SilMA can be crosslinked together via UV irradiating. (D) SEM of the cross section of GelMA, SilMA, and G-S hydrogel (Scale bar = 100 μm). (E) Pore diameter distribution of GelMA, SilMA and G-S hydrogel. (F) SEM of three concentration of GelMA hydrogel (Scale bar = 100 μm). (G) Pore diameter assessment of three concentration of GelMA hydrogel. Data represent mean ± SD; ***, $P < 0.001$.

hydrogels are synthesized by different methylation processes, they were still crosslinked together uniformly (Fig. 2C, video 1, supporting information). An investigation was conducted on the influence of SilMA content in G-S hydrogels on the acute wound healing.

3.2. Optimization of the composition of G-S hydrogel

Cell viability, attachment, and differentiation are largely influenced by the average pore size of a biological scaffold [32]. Micrometer pore sizes promote cellular attachment and proliferation [33], while macroscopic patterns with a minimum diameter of around 100 μm improve cell and capillary ingrowth [34]. It has been observed that pores around 100 μm in diameter are appropriate for skin tissue engineering [35]. A scanning electron microscope (SEM) was used to observe the microstructure in the hydrogel. The internal microstructures of GelMA, SilMA, and G-S hydrogel with the same concentration (4% w/v) were observed (Fig. 2D). In comparison with the single-network GelMA (163.78 ± 36.53 μm) and SilMA (125.16 ± 24.39 μm), the G-S hydrogel had smaller pore sizes (76.70 ± 20.02 μm), which may be due to the tight cross-linking of its dual-network structure (Fig. 2E). A disc construct was printed with different weight to volume ratios (3, 4, 5%) of GelMA hydrogel to determine the effect of the GelMA concentration on the pore size of G-S (Fig. 2F). With GelMA concentration increasing, the sizes of the pores decreased. The average pore sizes observed were 226.54 ± 41.86 μm (3% GelMA), 162.75 ± 15.44 μm (4% GelMA) and 82.76 ± 20.56 μm (5% GelMA) (Fig. 2G). After double crosslinking of SilMA and GelMA, the internal pore sizes of G-S were decreased (76.70 ± 20.02 μm). Since the larger pores will be benefit for cell adhesion and growth, we chose GelMA at 4% (w/v) with larger pores to approach the pore size around 100 μm in G-S hydrogel.

The gradients of SilMA concentration were adopted to optimize the concentration of SilMA that would be added in the G-S. This process evaluates the impact of SilMA content on G-S hydrogel in physicochemical properties and determines the synergistic effect of SilMA incorporated with GelMA for the improved physical properties. A cross-section of the produced G-S hydrogels after freeze-drying was observed with SEM. Fig. 3A shows that all G-S composite hydrogels exhibited a macroporous structure. The average pore diameters of 4%GelMA/4% GelMA (G:S = 1:0), 4%GelMA/4%SilMA (G:S = 1:1), 4%GelMA/8% SilMA (G:S = 1:2) and 4%GelMA/12%SilMA (G:S = 1:3) were 166.31 ± 31.61 μm, 121.79 ± 29.04 μm, 100.54 ± 14.53 μm and 48.37 ± 12.17 μm, respectively (Fig. 3B). It could be explained that the increased density of G-S after crosslink is correlated with the SilMA concentration. It seems that 4%GelMA/8%SilMA (G: S = 1:2) have the optimal pore size, which is beneficial to the cell adhesion and growth.

The bioengineered scaffolds must possess appropriate biomechanics properties that correlates with the tissue that will be replaced [36]. The mechanical properties of the G-S hydrogel can be adjusted by changing the concentration and ratio of the contained hydrogels. Physical characters of the hydrogels made of 4%GelMA/4%GelMA (G:S = 1:0), 4% GelMA/4%SilMA (G:S = 1:1), 4%GelMA/8%SilMA (G:S = 1:2) and 4% GelMA/12%SilMA (G:S = 1:3) were determined. Fig. 3C shows the dynamic change graph. The loss modulus (G″) is greater than the storage modulus (G′) prior to photo-crosslinking, and the G′ is greater than the G″ after 30 s of photo-crosslinking in all groups described above. In addition, as the proportion of SilMA in G-S hydrogel increases, the modulus of G-S

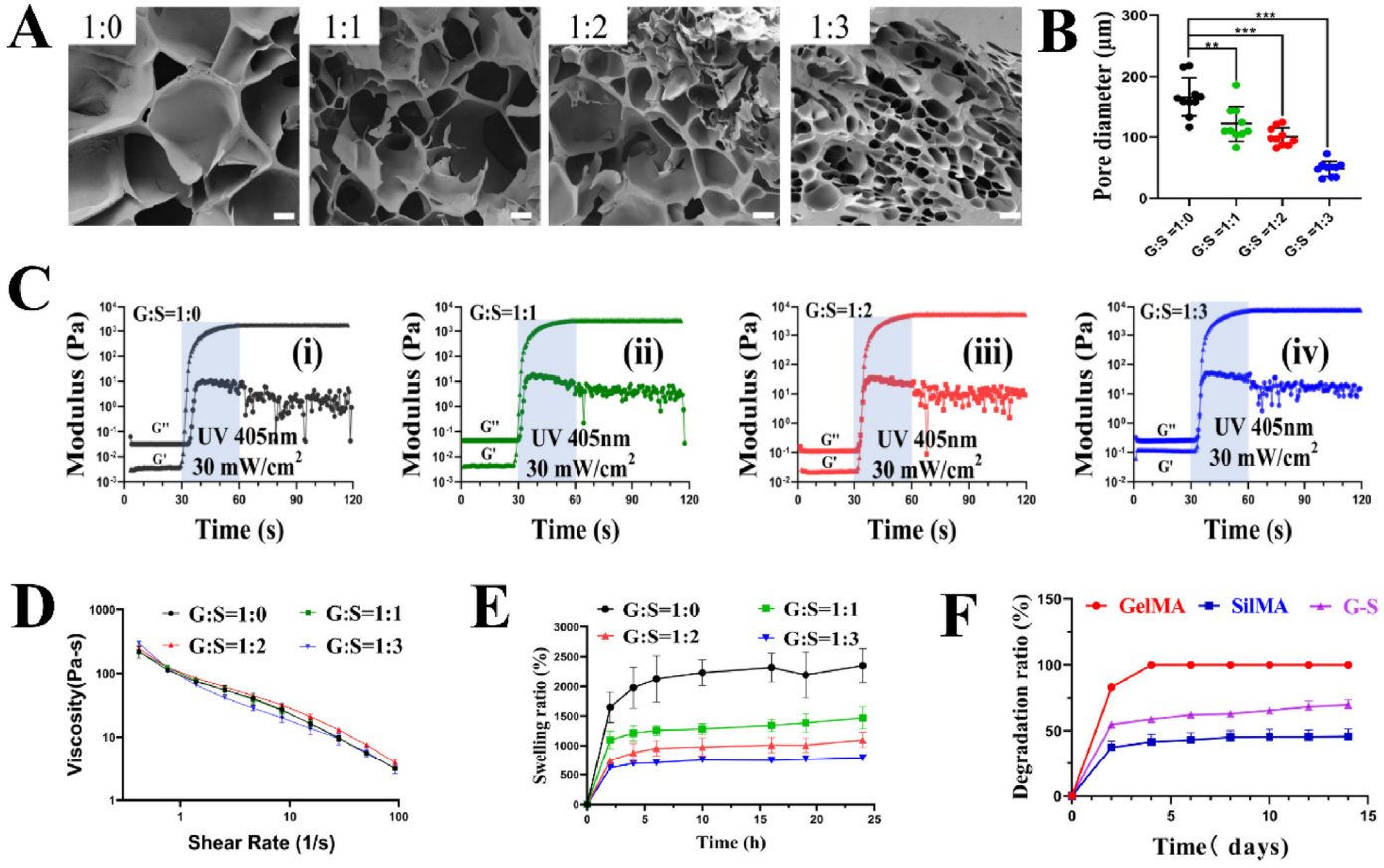

Fig. 3. (A) SEM observations of G-S hydrogel with four different ratios of gelatin and silk fibroin (Scale bar = 50 μm). (B) Pore diameter assessment of G-S hydrogel with four different ratios of gelatin and silk fibroin. (C) Rheological assessment of G-S hydrogel with four different ratios of gelatin and silk fibroin. (D) Viscosity of G-S hydrogel with four different ratios of gelatin and silk fibroin (n = 3). (E) Swelling ratio of G-S hydrogel with four different ratios of gelatin and silk fibroin. (F) Degradation of G-S hydrogel with four different ratios of gelatin and silk fibroin (n = 3). Data represent mean ± SD; **, $P < 0.01$, ***, $P < 0.001$.

hydrogel increases as well. It tells us that the mechanical properties of G-S are greatly enhanced by the addition of SilMA. Moreover, skin is well known to have great ductility, and G-S hydrogel can also be adjusted to obtain good ductility by adding SilMA (**Video 2**, supporting information).

The viscosity of hydrogels is a key determinant of their ability to be printed, especially for extrusion printing method. Ideally, the hydrogel must be able to shear thin to ensure the uniform extrusion of the product and a stable pressure within the cylinder [37]. As shown in Fig. 3D, A composite hydrogel with a higher SilMA content has a higher initial viscosity. However, there is no significant differences in the slopes of the curves and the rates of changing SilMA concentration among the groups with different composite hydrogels. The explanation might be that GelMA, a temperature-sensitive hydrogel, can keep the gelation only at below 25 °C; while SilMA is not sensitive to temperature. So different concentration of SilMA does not influence the outcome of viscosity tests. Results indicate that all the samples are capable of shear-thinning and can be used as a hydrogel for extrusion bioprinting.

In tissue engineering applications, the swelling characteristic is critical since it directly affects solute diffusion and mobility as well as mechanical properties. As shown in Figs. 3E and 4%GelMA reached swelling equilibrium in 10 h, while the different ratio G-S quickly reached the swelling equilibrium in 6 h. The swelling ratio of the four composite hydrogels were 2347.19 ± 286.59% (G:S = 1:0), 1467.37 ± 286.59% (G:S = 1:1), 1096.11 ± 130.46% (G:S = 1:2) and 790.76 ± 19.52% (G:S = 1:3), respectively. The findings demonstrate that the swelling ratio of composite hydrogel is increased when SilMA concentration is decreased. This can be explained because reduced volume of water in the solute as a consequence of adding SilMA [38].

The hydrogels used as biomaterials for tissue engineering structures must be of proper biodegradability and degradation rate. The main proteolytic enzyme involved in wound healing is type II collagenase (matrix metalloproteinase-8 [MMP-8]) [39]. It has been confirmed that GelMA is degraded by enzymes since gelatin contains sequences that collagenases can recognize [40]. The degradation of the hydrogels was assessed by immersing them in type II collagenase solution (2 U/mL). Fig. 3F shows the degradation profiles of different composite hydrogels within 2 weeks in vitro. The GelMA shows higher degradation, SilMA lower degradation and G-S between them. Within 1 week, the pure GelMA group degraded completely; while the weight loss in the groups of G: S = 1:1, G: S = 1:2, and G: S = 1:3 was less than 60%. Results indicate that the addition of SilMA resulted in a tightly connected internal network of the composite hydrogel. It is possibly due to intertwined GellMA and SilMA makes the G-S hydrogel more resistant to degradation. The degradation of type II collagenase solution-immersed G-S hydrogels was lasting longer than GelMA hydrogel due to the absence of MMP-sensitive motifs in SilMA. Thus, G-S hydrogel can maintain a moist healing environment in the wound bed for a long time with adequate degradation capacity, and is considered to be more suitable for skin wound dressing. The pore size, cell viability, cell growth state, swelling ratio, and mechanical properties were evaluated to optimize the portion of SilMA in G-S hydrogel. After comparing the results among the

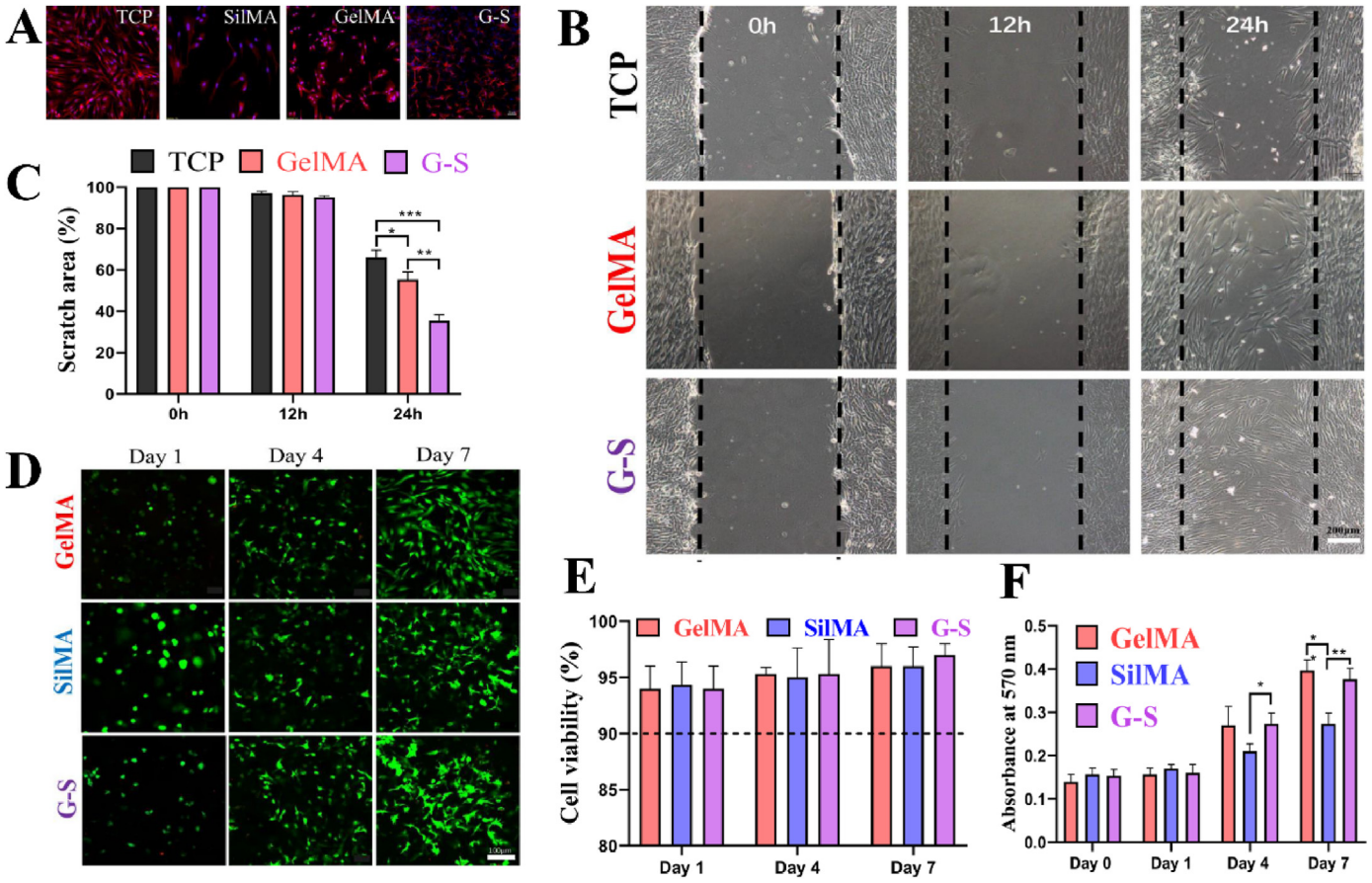

Fig. 4. (A) Cell adhesion on the surface of the control (TCP culture dishes), GelMA, SilMA, and G-S hydrogel (Scale bar = 50 μm). (B) Images of wound scratch migration assay in control, GelMA and G-S groups. (C) Quantification of fibroblast cells migration on TCP cell culture dish, GelMA coated, and G-S hydrogel coated dishes (n = 3) (Scale bar = 200 μm). (D) Cell viability assessment in 3D bioprinted skin pateches of GelMA, SilMA and G-S groups (Day 1, Day 4, Day 7). (E) Cell viability of GelMA, SilMA and G-S groups in day 1, day 4 and day 7. (F) Cell proliferation of GelMA, SilMA and G-S groups with MTT assay at days 1, 4, and 7. Data represent mean ± SD; *, $P < 0.05$, **, $P < 0.01$, ***, $P < 0.001$.

experimental groups, the combination of G: S = 1:2 shows the best outcomes. Therefore, we chose an optimized composition of 4% GelMA and 8% SilMA to create G-S hydrogel in this study.

3.3. Cell adhesion, migration, biocompatibility, and proliferation in vitro

Tissue engineering relies largely on the interaction between cells and biomaterials. Cell adhesion determines cell migration, proliferation, differentiation, and other essential cell behaviors, and forms the basis for communication between cells and their microenvironment [41]. GelMA has been widely used as a wound-healing agent due to its cell adhesion and MMP reactive peptide group [42]. As shown in Fig. 4A, In the incubation medium for 24 h, fibroblast cells adhered efficiently to GelMA and G-S hydrogels, which is similar with the cells adhering to the tissue culture polystyrene (TCP) culture dishes. It suggests that GelMA and G-S hydrogels can quickly promote the adhesion and growth of fibroblasts evenly (Fig. 1S, supporting information). Whereas the aggregation of fibroblasts was observed on SilMA that are significantly different from the cells on G-S (Fig. 2S, supporting information).

Inflammation, proliferation, and remodeling are the three phases of normal wound healing. Fibroblasts that proliferate and migrate into the wound bed are crucial in forming granulation tissue and promoting its contraction during the proliferative phase [43]. In the scratch test (Fig. 4B and C), the remaining blank area in G-S group was significantly lower than that in GelMA and TCP groups when treated time was increased from 12 to 24 h.

To fabricate 3D tissues or organs, 3D bioprinting uses biomaterials, specific cells, motion control, and computer-aided design software (CAD). Ideally, a bioink should be printable, biodegradable, and biocompatible to cells. The SilMA is not suitable for extrusion printer due to its low viscosity. Whereas gelatin, which degrades rapidly at 37 °C, is a common additive used in extrusion printing. In this study, the SilMA group is composed of 8% SilMA, the GelMA group is of 4% GelMA, and the G-S group is of 4% GelMA and 8%SilMA, respectively. Specifically, the ideal air pressure for achieving printability in extruding composite hydrogels precisely through the nozzles was determined in this study. To evaluate the biocompatibility of the bioprinted skin patches, fibroblast cells were mixed with the hydrogels before bioprinting, and then the cell viability and proliferation were analyzed. Live/Dead assays were performed to assess the cytotoxicity of fibroblast cells in various hydrogels. From the fluorescent images in Fig. 4D and **E**, it was found that cells spread out well and the viability of cells was over 90% after being cultured for 7 days in each hydrogel groups. There is no significant difference of living cells in all groups, which indicates that SilMA, GelMA, and G-S hydrogels have no potential cytotoxicity. Furthermore, the process of 3D bioprinting did not influence the cell viability greatly due to the air pressure being controlled below 100 kPa. The proliferation of fibroblast cells in bioprinted constructs was quantified by MTT assay at day 0, 1, 4, and 7 post-printing. As shown in Fig. 4F, cells cultured in the hydrogels exhibited excellent cell proliferation after being cultured for 4 days. The comparison between the G-S and SilMA groups suggests that the cell proliferation in SilMA hydrogel can be improved by the incorporation of GelMA hydrogel. Furthermore, there is no significance for cell proliferation between the G-S and GelMA groups.

Previous work confirmed that silk fibroin has excellent biological characteristics such as cell proliferation and low inflammation [44,45]. Gelatin can synergistically provide more adherent sites for cells in hydrogels, enabling a more favorable environment for cell adhesion, proliferation, and spreading [46]. Our study further confirmed that the main functions of silk fibroin and gelatin are not affected after the methylation process. The G-S hydrogel demonstrated superior capability of migration, cytocompatibility, and proliferation. Benefitting from the synergistic effect of GelMA and SilMA, G-S hydrogel exhibits excellent biological characteristics and could be a potential therapeutic material for wound healing.

3.4. Wound healing study in vivo

A full-thickness skin wound model was established to evaluate the wound healing efficacy of the G-S hydrogel in vivo. Printed skin patches were photo-crosslinked and placed in PBS for 24 h at 37 °C before being transplanted into mice. As shown in Fig. 5A, G-S hydrogel accelerated wound healing significantly compared to other treatments. A schematic diagram of Fig. 5B illustrates the dynamic healing process. The quantitative measurements of wound size have been summarized in Fig. 5C. On day 0, two circular wounds (diameter 8 mm) were created on the dorsal either side of spinal. The hydrogel patch was transplanted into the one site of wounds and the other site of wounds was treated with PBS only as the control group. The skin wounds were healing in a similar way that happens in human, including the processing of granulation hyperplasia and contraction, as well as re-epithelialization. Though contraction is a physiological response to skin injuries, excessive contraction may result in hypertrophic scarring, poor cosmetic results, and reduced functionality of the newly healed tissue [47]. In addition, the mechanical properties of the healing area with contracted scar are generally weaker than the original tissue, resulting in a higher risk of wound reopening [48]. Consequently, novel therapies aim to limit contractures [49]. On day 3, t the wound area contractures in the groups of Control, GelMA, SilMA, and G-S hydrogel were 53.57%, 62.50%, 42.97%, and 31.89%, respectively. The early contraction was found in the Control, GelMA, and SilMA groups by the wound size, but not in G-S group. Hence, the G-S hydrogel appears to be capable of inhibiting the contraction of skin. On day 7, the image analyses showed that wound healing ratio of 76.09% in GelMA, 77.41% in SilMA, and 79.67% in G-S group. The average wound sizes in G-S and SilMA group were smaller than that in GelMA group. The G-S hydrogel appears to be able to ease wound contracture at the early stage and to speed wound closure overall. The lower ratio of wound healing in GelMA group was possibly due to the rapid degradation of the GelMA in vivo. The wound healing rate in the Control group was the lowest, which did not surpass 70% healing within 7 days. The wounds treated with G-S hydrogel maintained the best healing statue among each group with increased time. On day 12, the G-S group has already fully healed, while the remaining groups still showed significant unhealed ratio of GelMA (3.31%), SilMA (2.72%), and Control group (4.35%), respectively (Fig. 5D). The above results reveal that the combination of SilMA and GelMA can promote wound healing in vivo.

The re-epithelialization process is the precursor to the healing of the dermis [50]. It serves to prevent excessive transdermal water loss and wound infections by establishing a functional barrier at an early stage during wound healing. The regenerated epithelium was evaluated by quantifying the length of neo-epithelial tongue and area of neo-epithelium. On day 7, since the wounds had not healed completely, the trauma edge was used to determine its extent (Fig. 6A). Compared to GelMA group, G-S or SilMA group showed significantly better wound healing. As further confirmation, examination of hematoxylin-eosin (H&E) staining was performed to investigate the structure of wound beds and progress of epithelization. Quantitative measurements of wound cross-sectional thickness confirmed this result with the length of neo-epithelial tongue of the Control (10.08 ± 1.61 mm), GelMA (13.78 ± 1.32 mm), SilMA (16.38 ± 0.84 mm), and G-S group (22.80 ± 2.02 mm), respectively (Fig. 6B). Furthermore, the area of neo-epithelium of the Control (11.54 ± 1.31 mm^2), GelMA (15.60 ± 0.54 mm^2), SilMA (18.56 ± 0.70 mm^2), and G-S group (32.33 ± 2.79 mm^2), respectively (Fig. 6C). In addition, further confirmation was accomplished using proliferating cell nuclear antigen (PCNA) staining (Fig. 6D). As shown in Fig. 6E, quantitative measurement of the relative PCNA of four groups were 1, 1.32 ± 0.04, 2.35 ± 0.12, 3.33 ± 0.09, respectively. On day 9, the tissue sections of the wounds in the G-S group showed relatively complete epithelium, while the wounds treated by SilMA, GelMA, and PBS demonstrated incomplete epithelium. On day 12, the G-S hydrogel group exhibited the best epithelialization among experimental groups significantly (Fig. 7A). The H&E staining was confirmed the above observation

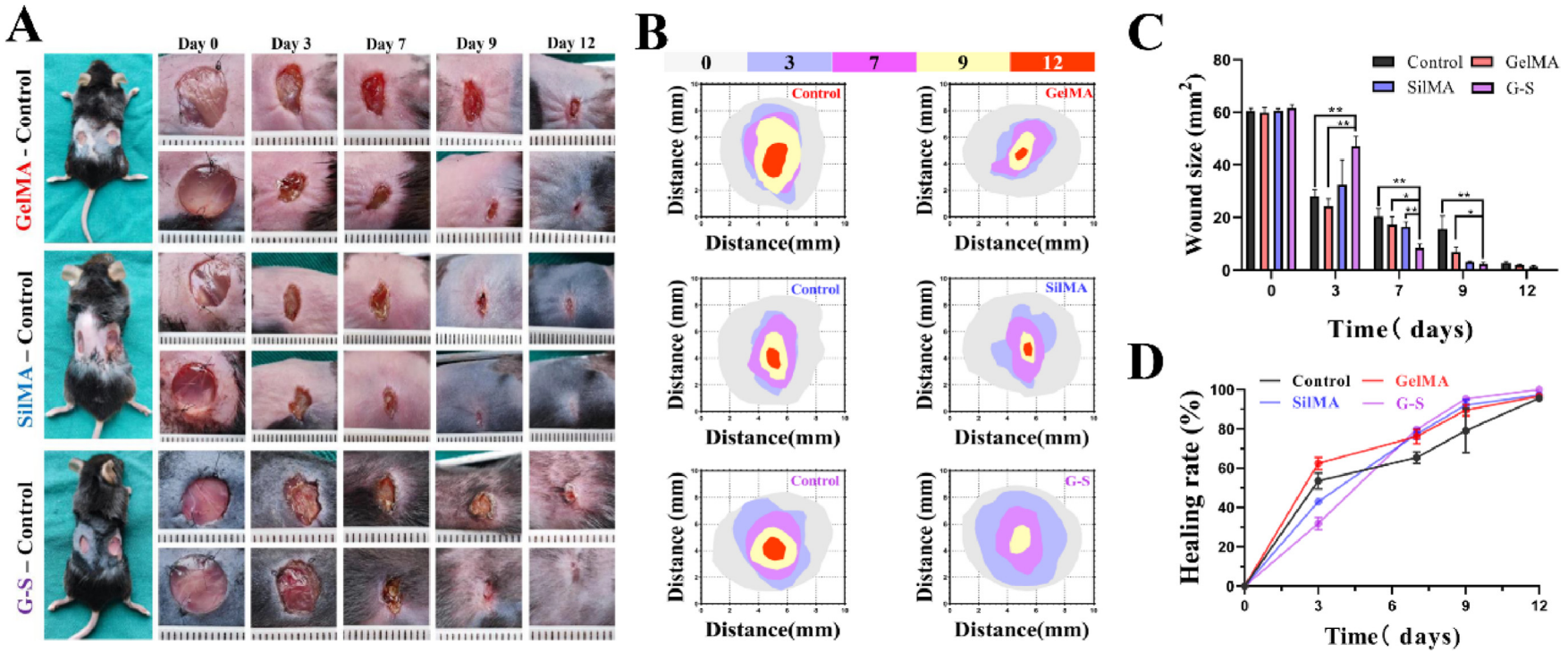

Fig. 5. (A) Representative images of wound healing process in mice in GelMA, SilMA and G-S groups. (B) Schematic diagram of the wound managed by different treatments in 12 days. (C) Quantitative data of wound size at different time points (n = 3). (D) Quantitative data of wound healing ratio at different time points (n = 3). Data represent mean ± SD; *, $P < 0.05$, **, $P < 0.01$.

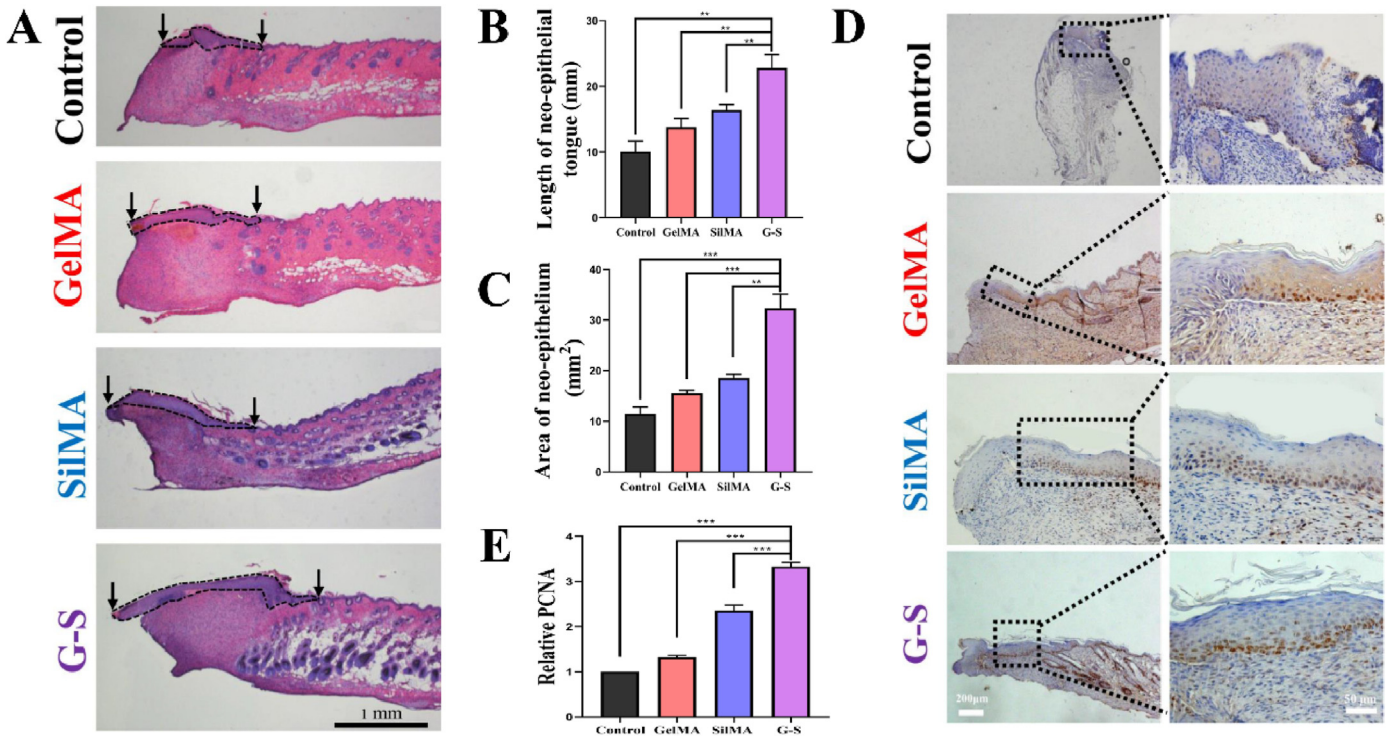

Fig. 6. (A) Representative images of wound tissue sections in different treatment groups stained by H&E on day 7 (Scale bar = 1 mm and 50 μm). (B) Quantification of the length of neo-epithelial tongue in different treatment groups on day 7 (n = 3). (C) Quantification of the area of neo-epithelium in different treatment groups on day 7 (n = 3). (D) Representative images of wound tissue sections stained by proliferating cell nuclear antigen (PCNA) in different treatment groups on day 7 (Scale bar = 1 mm and 50 μm). (E) Quantification of the relative PCNA staining in different treatment groups on day 7 (n = 3). Data represent mean ± SD; *, $P < 0.05$, **, $P < 0.01$, ***, $P < 0.001$.

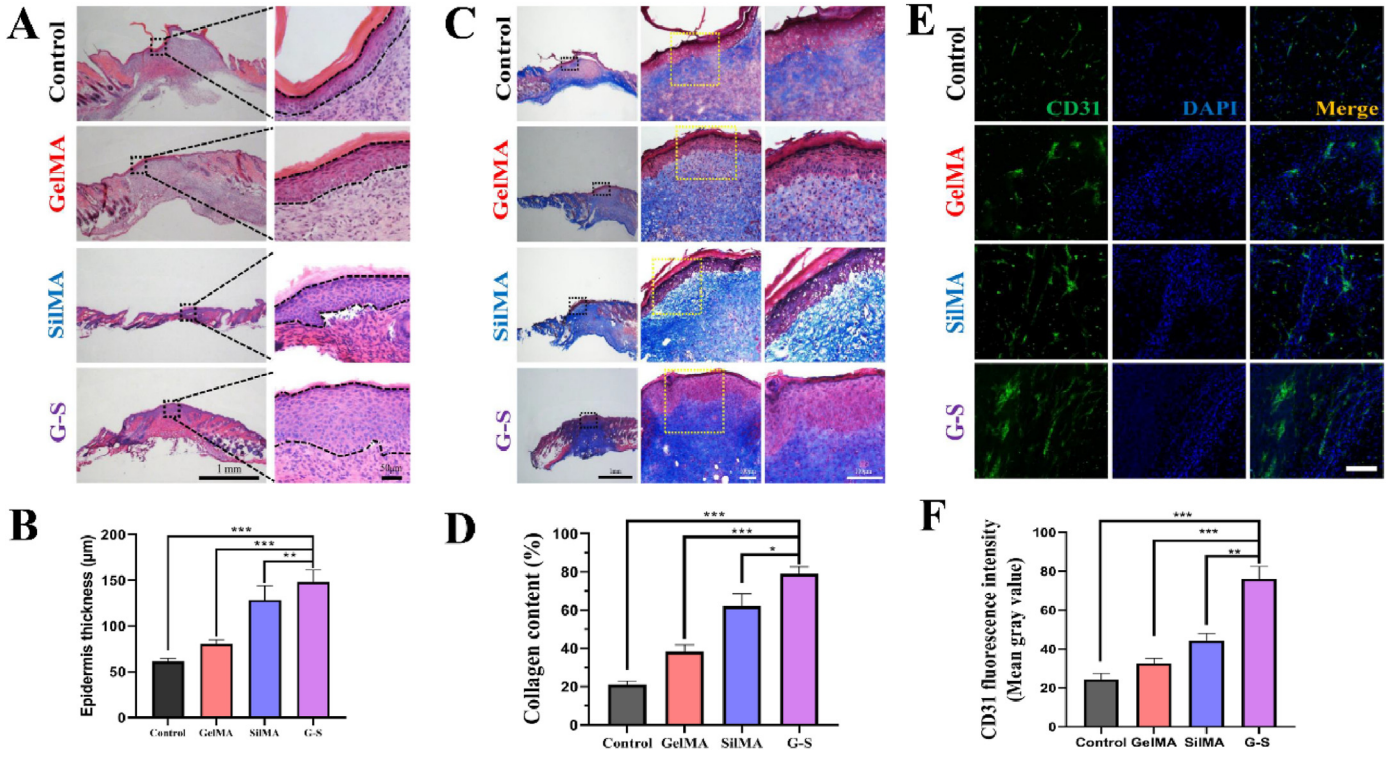

Fig. 7. (A) Representative images of wound tissue sections stained by H&E in different treatment groups on day 12 (Scale bar = 1 mm and 50 μm). (B) Quantification of the epidermis thickness in different treatment groups on day 12 (n = 3). (C) Images of collagen deposition by Masson's trichrome staining in different treatment groups on day 12 post treatment (Scale bar = 1 mm and 100 μm). (D) Quantification of collagen deposition density in different treatment groups on day 12 (n = 3). (E) Representative images of wound tissue sections stained by CD31 in different treatment groups on day 12 (Scale bar = 100 μm). (F) Quantification of the relative CD31 staining in different treatment groups on day 7 (n = 3). Data represent mean ± SD; *, $P < 0.05$, **, $P < 0.01$, ***, $P < 0.001$.

by quantifying neo-epidermal thickness with the neo-epidermal thickness of 61.39 ± 1.02 μm in Control, 80.23 ± 2.68 μm GelMA, 128.47 ± 12.61 μm in SilMA, and 147.94 ± 17.37 μm in G-S group, respectively (Fig. 7B).

Wound healing is dependent on collagen deposition and cell growth [51]. Masson's trichrome staining results revealed that the G-S hydrogel group showed the highest collagen fiber density in the wound bed after 12 days compared to the other groups (Fig. 7C). These findings suggest that the amount of ECM deposited in the wound bed following G-S treatment has been remarkably increased. Quantitative measurements of collagen deposition were performed with the results of 21% in Control, 38.33% in GelMA, 62% in SilMA, and 79% in G-S group (Fig. 7D). As shown in Fig. 7E, the expression of CD31 in G-S hydrogel group was higher than other groups, which indicates that more mature capillaries were cumulated in the wound bed in G-S group. Also, the CD31 fluorescence intensity in G-S hydrogel group was significantly increased compared with other groups (Fig. 7F), which means that the advantages of dual crosslinkable G-S hydrogel may promote angiogenesis in wound area.

GelMA hydrogel does show cell adhesion. However, GelMA has a low fracture energy and is susceptible to cracks [52]. In addition, GelMA hydrogel swells and degrades gradually as a result of being transplanted into the wound area will decline the mechanical properties further by over time. Therefore, despite its higher biocompatibility and cell adhesion ability, GelMA could not support the entire healing process mechanically and structurally. The addition of SilMA to GelMA forms a dual-crosslinked G-S hydrogel that is less prone to fracture, slows proper degradation, and supports the entire wound healing process. Our investigation indicates that G-S hydrogel may achieve the requirement for treating skin wound based on the experimental outcomes such as faster wound closure, angiogenesis, tissue regeneration, as well as the safety in use.

4. Conclusion

We have developed a hybrid hydrogel of GelSilMA, which incorporates photo-crosslinkable Silk fibroin and gelatin prepolymers modified with the reactive methacrylate groups. The G-S hydrogel is gelatinized by UV crosslinking in just one step, which results the dual-crosslinking actions among GelMA and SilMA synchronously. The G-S hydrogel exhibits higher porous, biodegradable, and adjustable mechanical properties. The intrinsic dual modulation efficacy of G-S hydrogel could guide skin wound healing in bio-therapeutical way. We found that G-S hydrogel could increase fibroblast migration, proliferation, and adhesion effectively in vitro. Animal study confirmed the effectiveness of G-S hydrogel in promoting skin wound healing. The G-S hydrogel is of the better biological and mechanical properties than a single network of GelMA or SilMA. Taken together, the G-S hydrogel presents its therapeutic potential for the management of acute skin wound.

Author statement

Lei Xu: Conceptualization, Methodology, Investigation, Data curation, Formal analysis, Visualization, Writing – original draft, Writing – review & editing; **Zhiqiang Zhang**: Methodology, Investigation, Data curation, Writing – review & editing; **Adam M Jorgensen:** Methodology, Investigation; **Yuan Yang:** Investigation, Data curation; **Qianheng Jin:** Investigation; **Guangliang Zhang:** Methodology, Funding acquisition; **Gaobiao Cao:** Investigation; **Yi Fu:** Methodology, Investigation; **Weixin Zhao:** Supervision; Writing – review & editing; **Jihui Ju:** Project administration, Funding acquisition, Supervision, Writing – review & editing; **Ruixing Hou:** Project administration, Funding acquisition, Supervision, Writing – review & editing..

Declaration of competing interest

The authors declare that they have no known competing financial interests or personal relationships that could have appeared to influence the work reported in this paper.

Data availability

Data will be made available on request.

Acknowledgements

This research was funded by a grant from Suzhou Minsheng Technology (SYS2020070), Natural Science Foundation of Jiangsu Province (BK20221245) and Suzhou Key Disciplines (SZXK202127).

Appendix A. Supplementary data

Supplementary data to this article can be found online at https://doi.org/10.1016/j.mtbio.2023.100550.

References

[1] R. Jin, Y. Cui, H. Chen, Z. Zhang, T. Weng, S. Xia, M. Yu, W. Zhang, J. Shao, M. Yang, C. Han, X. Wang, Three-dimensional bioprinting of a full-thickness functional skin model using acellular dermal matrix and gelatin methacrylamide bioink, Acta Biomater. 131 (2021) 248–261.
[2] S. Krishtul, L. Baruch, M. Machluf, Processed tissue-derived extracellular matrices: tailored platforms empowering diverse therapeutic applications, Adv. Funct. Mater. 30 (2019), 1900386.
[3] S. Wu, Z. Xiao, J. Song, M. Li, W. Li, Evaluation of BMP-2 enhances the osteoblast differentiation of human amnion mesenchymal stem cells seeded on nano-hydroxyapatite/collagen/poly(l-lactide), Int. J. Mol. Sci. 19 (8) (2018) 2171.
[4] T.D. Johnson, R.C. Hill, M. Dzieciatkowska, V. Nigam, A. Behfar, K.L. Christman, K.C. Hansen, Quantification of decellularized human myocardial matrix: a comparison of six patients, Proteonomics Clin. Appl. 10 (1) (2016) 75–83.
[5] K. Las Heras, M. Igartua, E. Santos-Vizcaino, R.M. Hernandez, Chronic wounds: current status, available strategies and emerging therapeutic solutions, J. Contr. Release 328 (2020) 532–550.
[6] A.M. Jorgensen, M. Varkey, A. Gorkun, C. Clouse, L. Xu, Z. Chou, S.V. Murphy, J. Molnar, S.J. Lee, J.J. Yoo, S. Soker, A. Atala, Bioprinted skin recapitulates normal collagen remodeling in full-thickness wounds, Tissue Eng. 26 (9–10) (2020) 512–526.
[7] Y. Wang, F. Lu, E. Hu, K. Yu, J. Li, R. Bao, F. Dai, G. Lan, R. Xie, Biogenetic acellular dermal matrix maintaining rich interconnected microchannels for accelerated tissue amendment, ACS Appl. Mater. Interfaces 13 (14) (2021) 16048–16061.
[8] Y. Wang, X. Yuan, B. Yao, S. Zhu, P. Zhu, S. Huang, Tailoring bioinks of extrusion-based bioprinting for cutaneous wound healing, Bioact. Mater. 17 (2022) 178–194.
[9] S. Van Belleghem, B. Mahadik, K. Snodderly, Z. Mote, B. Jiang, J.R. Yu, S. McLoughlin, X. He, A.J. Nam, J.P. Fisher, Dual extrusion patterning drives tissue development aesthetics and shape retention in 3D printed nipple-areola constructs, Adv Healthc Mater 10 (23) (2021), e2101249.
[10] A.M. Jorgensen, J.J. Yoo, A. Atala, Solid organ bioprinting: strategies to achieve organ function, Chem. Rev. 120 (19) (2020) 11093–11127.
[11] Y. Liu, M.B. Chan-Park, A biomimetic hydrogel based on methacrylated dextran-graft-lysine and gelatin for 3D smooth muscle cell culture, Biomaterials 31 (6) (2010) 1158–1170.
[12] P.E. Van den Steen, B. Dubois, I. Nelissen, P.M. Rudd, R.A. Dwek, G. Opdenakker, Biochemistry and molecular biology of gelatinase B or matrix metalloproteinase-9 (MMP-9), Crit. Rev. Biochem. Mol. Biol. 37 (6) (2002) 375–536.
[13] L. Xu, M. Varkey, A. Jorgensen, J. Ju, Q. Jin, J.H. Park, Y. Fu, G. Zhang, D. Ke, W. Zhao, R. Hou, A. Atala, Bioprinting small diameter blood vessel constructs with an endothelial and smooth muscle cell bilayer in a single step, Biofabrication 12 (4) (2020), 045012.
[14] N.W. Chai, J.T. Zhang, Q.Q. Zhang, H.B. Du, X. He, J. Yang, X.J. Zhou, J.W. He, C.L. He, Construction of 3D printed constructs based on microfluidic microgel for bone regeneration, Compos. B Eng. 223 (2021), 109100.
[15] H. Stratesteffen, M. Köpf, F. Kreimendahl, A. Blaeser, S. Jockenhoevel, H. Fischer, GelMA-collagen blends enable drop-on-demand 3D printablility and promote angiogenesis, Biofabrication 9 (4) (2017), 045002.
[16] J. Yin, M. Yan, Y. Wang, J. Fu, H. Suo, 3D bioprinting of low-concentration cell-laden gelatin methacrylate (GelMA) bioinks with a two-step cross-linking strategy, ACS Appl. Mater. Interfaces 10 (8) (2018) 6849–6857.
[17] Y. Qi, H. Wang, K. Wei, Y. Yang, R.Y. Zheng, I.S. Kim, K.Q. Zhang, A review of structure construction of silk fibroin biomaterials from single structures to multi-level structures, Int. J. Mol. Sci. 18 (3) (2017) 237.
[18] S.H. Kim, D.Y. Kim, T.H. Lim, C.H. Park, Silk fibroin bioinks for digital light processing (DLP) 3D bioprinting, Adv. Exp. Med. Biol. 1249 (2020) 53–66.

[19] W. Zhu, Y. Dong, P. Xu, Q. Pan, K. Jia, P. Jin, M. Zhou, Y. Xu, R. Guo, B. Cheng, A composite hydrogel containing resveratrol-laden nanoparticles and platelet-derived extracellular vesicles promotes wound healing in diabetic mice, Acta Biomater. 154 (2022) 212–230.
[20] S.H. Kim, Y.K. Yeon, J.M. Lee, J.R. Chao, Y.J. Lee, Y.B. Seo, M.T. Sultan, O.J. Lee, J.S. Lee, S.I. Yoon, I.S. Hong, G. Khang, S.J. Lee, Y.Y. Yoo, C.H. Park, Precisely printable and biocompatible silk fibroin bioink for digital light processing 3D printing, Nat. Commun. 9 (1) (2018) 1620.
[21] H. Hong, Y.B. Seo, D.Y. Kim, J.S. Lee, Y.J. Lee, H. Lee, O. Ajiteru, M.T. Sultan, O.J. Lee, S.H. Kim, C.H. Park, Digital light processing 3D printed silk fibroin hydrogel for cartilage tissue engineering, Biomaterials 232 (2020), 119679.
[22] S.H. Kim, H. Hong, O. Ajiteru, M.T. Sultan, Y.J. Lee, J.S. Lee, O.J. Lee, H. Lee, H.S. Park, K.Y. Choi, J.S. Lee, H.W. Ju, I.S. Hong, C.H. Park, 3D bioprinted silk fibroin hydrogels for tissue engineering, Nat. Protoc. 16 (12) (2021) 5484–5532.
[23] W. Zhu, Y. Dong, P. Xu, Q. Pan, K. Jia, P. Jin, M. Zhou, Y. Xu, R. Guo, B. Cheng, A composite hydrogel containing resveratrol-laden nanoparticles and platelet-derived extracellular vesicles promotes wound healing in diabetic mice, Acta Biomater. 154 (2022) 212–230.
[24] K. Yue, G. Trujillo-de Santiago, M.M. Alvarez, A. Tamayol, N. Annabi, A. Khademhosseini, Synthesis, properties, and biomedical applications of gelatin methacryloyl (GelMA) hydrogels, Biomaterials 73 (2015) 254–271.
[25] M. Ali, A.K. Pr, J.J. Yoo, F. Zahran, A. Atala, S.J. Lee, A photo-crosslinkable kidney ECM-derived bioink accelerates renal tissue formation, Adv Healthc Mater 8 (7) (2019), e1800992.
[26] I. Pepelanova, K. Kruppa, T. Scheper, A. Lavrentieva, Gelatin-methacryloyl (GelMA) hydrogels with defined degree of functionalization as a versatile toolkit for 3D cell culture and extrusion bioprinting, Bioengineering (Basel) 5 (3) (2018) 55.
[27] F. Wang, Y. Wang, C. Tian, S. Xu, R. Wang, K. Hou, W. Chen, P. Zhao, L. Yu, Z. Lu, D.L. Kaplan, Q. Xia, Fabrication of the FGF1-functionalized sericin hydrogels with cell proliferation activity for biomedical application using genetically engineered Bombyx mori (B. mori) silk, Acta Biomater. 79 (2018) 239–252.
[28] A. Gaspar-Pintiliescu, A.M. Stanciuc, O. Craciunescu, Natural composite dressings based on collagen, gelatin and plant bioactive compounds for wound healing: a review, Int. J. Biol. Macromol. 138 (2019) 854–865.
[29] H. Hu, F.J. Xu, Rational design and latest advances of polysaccharide-based hydrogels for wound healing, Biomater. Sci. 8 (8) (2020) 2084–2101.
[30] Y. Liu, M.B. Chan-Park, A biomimetic hydrogel based on methacrylated dextran-graft-lysine and gelatin for 3D smooth muscle cell culture, Biomaterials 31 (6) (2010) 1158–1170.
[31] J. Vandooren, P.E. Van den Steen, G. Opdenakker, Biochemistry and molecular biology of gelatinase B or matrix metalloproteinase-9 (MMP-9): the next decade, Crit. Rev. Biochem. Mol. Biol. 48 (3) (2013) 222–272.
[32] Z. Li, K.M. Bratlie, The influence of polysaccharides-based material on macrophage phenotypes, Macromol. Biosci. 21 (8) (2021), e2100031.
[33] P.X. Ma, J.W. Choi, Biodegradable polymer scaffolds with well-defined interconnected spherical pore network, Tissue Eng. 7 (1) (2001) 23–33.
[34] V.J. Chen, P.X. Ma, Nano-fibrous poly (L-lactic acid) scaffolds with interconnected spherical macropores, Biomaterials 25 (11) (2004) 2065–2073.
[35] I.V. Yannas, E. Lee, D.P. Orgill, E.M. Skrabut, G.F. Murphy, Synthesis and characterization of a model extracellular matrix that induces partial regeneration of adult mammalian skin, Proc. Natl. Acad. Sci. U. S. A. 86 (3) (1989) 933–937.
[36] X. Zhao, Q. Lang, L. Yildirimer, Z.Y. Lin, W. Cui, N. Annabi, K.W. Ng, M.R. Dokmeci, A.M. Ghaemmaghami, A. Khademhosseini, Photocrosslinkable gelatin hydrogel for epidermal tissue engineering, Adv Healthc Mater 5 (1) (2016) 108–118.
[37] C. Mandrycky, Z. Wang, K. Kim, D.H. Kim, 3D bioprinting for engineering complex tissues, Biotechnol. Adv. 34 (4) (2016) 422–434.
[38] W. Xiao, J. He, J.W. Nichol, L. Wang, C.B. Hutson, B. Wang, Y. Du, H. Fan, A. Khademhosseini, Synthesis and characterization of photocrosslinkable gelatin and silk fibroin interpenetrating polymer network hydrogels, Acta Biomater. 7 (6) (2011) 2384–2393.
[39] B.C. Nwomeh, H.X. Liang, I.K. Cohen, D.R. Yager, MMP-8 is the predominant collagenase in healing wounds and nonhealing ulcers, J. Surg. Res. 81 (2) (1999) 189–195.
[40] X. Zhao, Q. Lang, L. Yildirimer, Z.Y. Lin, W. Cui, N. Annabi, K.W. Ng, M.R. Dokmeci, A.M. Ghaemmaghami, A. Khademhosseini, Photocrosslinkable gelatin hydrogel for epidermal tissue engineering, Adv Healthc Mater 5 (1) (2016) 108–118.
[41] Y. Bao, L. Wang, L. Shi, F. Yun, X. Liu, Y. Chen, C. Chen, Y. Ren, Y. Jia, Transcriptome profiling revealed multiple genes and ECM-receptor interaction pathways that may be associated with breast cancer, Cell. Mol. Biol. Lett. 24 (2019) 38.
[42] Z.M. Yang, X.H. Ren, Y. Liu, N-halamine modified ceria nanoparticles: antibacterial response and accelerated wound healing application via a 3D printed scaffold, Compos. B Eng. 227 (2021), 109390.
[43] J. Qu, X. Zhao, Y. Liang, T. Zhang, P.X. Ma, B. Guo, Antibacterial adhesive injectable hydrogels with rapid self-healing, extensibility and compressibility as wound dressing for joints skin wound healing, Biomaterials 183 (2018) 185–199.
[44] L. Meinel, S. Hofmann, V. Karageorgiou, C. Kirker-Head, J. McCool, G. Gronowicz, L. Zichner, R. Langer, G. Vunjak-Novakovic, D.L. Kaplan, The inflammatory responses to silk films in vitro and in vivo, Biomaterials 26 (2) (2005) 147–155.
[45] J.R. Mauney, T. Nguyen, K. Gillen, C. Kirker-Head, J.M. Gimble, D.L. Kaplan, Engineering adipose-like tissue in vitro and in vivo utilizing human bone marrow and adipose-derived mesenchymal stem cells with silk fibroin 3D scaffolds, Biomaterials 28 (35) (2007) 5280–5290.
[46] M. Sun, X. Sun, Z. Wang, S. Guo, G. Yu, H. Yang, Synthesis and properties of gelatin methacryloyl (GelMA) hydrogels and their recent applications in load-bearing tissue, Polymers 10 (11) (2018) 1290.
[47] J.J. Tomasek, G. Gabbiani, B. Hinz, C. Chaponnier, R.A. Brown, Myofibroblasts and mechano-regulation of connective tissue remodelling, Nat. Rev. Mol. Cell Biol. 3 (5) (2002) 349–363.
[48] D.T. Corr, D.A. Hart, Biomechanics of scar tissue and uninjured skin, Adv. Wound Care 2 (2) (2013) 37–43.
[49] K. Nuutila, A. Laukkanen, A. Lindford, S. Juteau, M. Nuopponen, J. Vuola, E. Kankuri, Inhibition of skin wound contraction by nanofibrillar cellulose hydrogel, Plast. Reconstr. Surg. 141 (3) (2018) 357e–366e.
[50] X. Zhao, Q. Lang, L. Yildirimer, Z.Y. Lin, W. Cui, N. Annabi, K.W. Ng, M.R. Dokmeci, A.M. Ghaemmaghami, A. Khademhosseini, Photocrosslinkable gelatin hydrogel for epidermal tissue engineering, Adv Healthc Mater 5 (1) (2016) 108–118.
[51] R. Huang, X. Zhang, W. Li, L. Shang, H. Wang, Y. Zhao, Suction cups-inspired adhesive patch with tailorable patterns for versatile wound healing, Adv. Sci. 8 (17) (2021), e2100201.
[52] A. Kalra, A. Lowe, A.M. Al-Jumaily, Mechanical behaviour of skin: a review, J. Mater. Sci. Eng. 5 (4) (2016), 1000254.